AGU PUBLICATIONS

Geophysical Research Letters

RESEARCH LETTER
10.1002/2016GL067843

Key Points:
- GOSAT estimated CO_2 abundance due to large emitters compared to inventory-based estimate
- Observed and inventory-based CO_2 abundance agree well over global and subcontinental scales
- Observation-model discrepancy (22%) over East Asia is close to uncertainty in emission inventory

Supporting Information:
- Supporting Information S1

Correspondence to:
R. Janardanan,
rajesh.janardanan@nies.go.jp

Citation:
Janardanan, R., S. Maksyutov, T. Oda, M. Saito, J. W. Kaiser, A. Ganshin, A. Stohl, T. Matsunaga, Y. Yoshida, and T. Yokota (2016), Comparing GOSAT observations of localized CO_2 enhancements by large emitters with inventory-based estimates, *Geophys. Res. Lett.*, *43*, 3486–3493, doi:10.1002/2016GL067843.

Received 18 JAN 2016
Accepted 2 MAR 2016
Accepted article online 9 MAR 2016
Published online 2 APR 2016

Comparing GOSAT observations of localized CO_2 enhancements by large emitters with inventory-based estimates

Rajesh Janardanan[1], Shamil Maksyutov[1], Tomohiro Oda[2,3], Makoto Saito[1], Johannes W. Kaiser[4], Alexander Ganshin[5,6], Andreas Stohl[7], Tsuneo Matsunaga[8], Yukio Yoshida[1], and Tatsuya Yokota[1]

[1]Center for Global Environmental Research, National Institute for Environmental Studies, Tsukuba, Japan, [2]Global Modeling and Assimilation Office, NASA Goddard Space Flight Center, Greenbelt, Maryland, USA, [3]Goddard Earth Science Technologies and Research, Universities Space Research Association, Columbia, Maryland, USA, [4]Max Planck Institute for Chemistry, Mainz, Germany, [5]Central Aerological Observatory, Dolgoprudny, Russia, [6]Tomsk State University, Tomsk, Russia, [7]NILU-Norwegian Institute for Air Research, Kjeller, Norway, [8]Center for Environmental Measurement and Analysis, National Institute for Environmental Studies, Tsukuba, Japan

Abstract We employed an atmospheric transport model to attribute column-averaged CO_2 mixing ratios (X_{CO2}) observed by Greenhouse gases Observing SATellite (GOSAT) to emissions due to large sources such as megacities and power plants. X_{CO2} enhancements estimated from observations were compared to model simulations implemented at the spatial resolution of the satellite observation footprint ($0.1° \times 0.1°$). We found that the simulated X_{CO2} enhancements agree with the observed over several continental regions across the globe, for example, for North America with an observation to simulation ratio of 1.05 ± 0.38 ($p < 0.1$), but with a larger ratio over East Asia (1.22 ± 0.32; $p < 0.05$). The obtained observation-model discrepancy (22%) for East Asia is comparable to the uncertainties in Chinese emission inventories (~15%) suggested by recent reports. Our results suggest that by increasing the number of observations around emission sources, satellite instruments like GOSAT can provide a tool for detecting biases in reported emission inventories.

1. Introduction

Monitoring CO_2 emissions from human activities is essential for verifying the efficiency of emission reduction efforts. The present estimates of the emissions of anthropogenic greenhouse gases are primarily based on bottom-up inventories based on statistical data [*Reuter et al.*, 2014]. Inconsistencies between underlying country-level statistics of energy use and inaccuracies in the use of these data cause poorly quantified errors in bottom-up emission inventories [*Guan et al.*, 2012; *Andres et al.*, 2012]. To quantify their errors, emission inventories need verification against independent atmospheric composition data [*National Research Council*, 2010; *Nisbet and Weiss*, 2010]. While ground-based observation networks are often too sparse for monitoring these emissions, satellite observations can alleviate this limitation [*Duren and Miller*, 2012]. Recent studies on estimating X_{CO2} abundance caused by fossil fuel CO_2 emissions from large point sources such as power plants [*Bovensmann et al.*, 2010] and localized areas of high emissions such as large cities [*Kort et al.*, 2012] are steps toward this goal. A recent study by *Kort et al.* [2012] has shown the capacity of Greenhouse gases Observing SATellite (GOSAT) observations [*Kuze et al.*, 2009; *Yokota et al.*, 2009; *Yoshida et al.*, 2013] to detect anthropogenic CO_2 emission signatures for megacities such as Los Angeles and Mumbai. They suggest that X_{CO2} enhancements due to megacity fossil fuel emissions can be as high as 3 ppm over cities like Los Angeles, large enough to be detected by satellite. However, those studies were confined to few locations due to the limited number of suitable observations. Here we analyze large volumes of GOSAT X_{CO2} data for concentration enhancements due to anthropogenic emissions from large sources around the globe and relate them to X_{CO2} enhancements simulated by a high-resolution transport model.

2. Data

2.1. GOSAT X_{CO2} Observations

In this study we used the National Institute for Environmental Studies GOSAT short wavelength infrared X_{CO2} Level 2 product (version 02.11, downloaded from https://data.gosat.nies.go.jp/) over the period from June 2009 to December 2012. To increase the chances of observing fossil fuel CO_2 emission signatures from large

point sources, we placed GOSAT target mode observation requests to the GOSAT Project Office, requesting 1500 target mode observations per month. The GOSAT data used here were subjected to a standard filtering and screening applied for general distribution. Further details on retrieval and quality assurance can be referred to in *Yoshida et al*. [2013].

2.2. Emission From Fossil Fuel

The fossil fuel CO_2 emission data used are the Open-source Data Inventory for Atmospheric Carbon dioxide (ODIAC) [*Oda and Maksyutov*, 2011]. This inventory of anthropogenic CO_2 emission is a global 1×1 km fossil fuel CO_2 emission inventory based on country-level fuel consumption, a global power plant database and satellite observations of night lights, remapped to 0.1° spatial grids as fossil fuel CO_2 emission fields in this study. National annual total CO_2 emissions were estimated using British Petroleum (BP's) fuel consumption statistics for coal, oil, and natural gas. The spatial distribution of point emissions was determined using power plant locations included in the CARbon Monitoring for Action (CARMA) power plant database (available at http://www.carma.org/), and nightlight distributions were used as proxy for emissions from sources other than power plants. It should be noted here that recently reported revisions in Chinese fossil fuel usage (for example, *Liu et al*. [2015] and China Energy Statistical Yearbooks) have not been accounted for in the emission inventory. Further details can be found in *Oda and Maksyutov* [2011].

2.3. Emission From Large-Scale Biomass Burning

To correct for the contribution to CO_2 emission from biomass burning in the GOSAT X_{CO2} ($\Delta X_{CO2,fire}$), we performed Lagrangian retroplume simulation with fire emissions prescribed by the Global Fire Assimilation System (GFAS version 1.1, [*Kaiser et al*., 2012]). In this product, the fire radiative power from Moderate Resolution Imaging Spectroradiometer (MODIS) on the Aqua and Terra satellites is assimilated and biomass burning CO_2 emissions are calculated using conversion factors for fire radiative power to biomass burning rate for different vegetation types. Observation gaps due to clouds are corrected for, and false observations corresponding to volcanic and industrial activities are eliminated. The daily emissions of CO_2 are prepared at a global spatial resolution of $0.1° \times 0.1°$.

2.4. Biospheric Fluxes

The influence of terrestrial biospheric CO_2 fluxes on X_{CO2} ($\Delta X_{CO2,bio}$) is estimated in a similar way using the Vegetation Integrative Simulator of Trace gases (VISIT) [*Ito*, 2010; *Saito et al*., 2014]. Global vegetation types are classified into 15 biomes in this model based on MODIS land cover data [*Friedl et al*., 2002]. The meteorological reanalysis data used to drive VISIT were taken from the Japanese 25 year reanalysis (JRA-25)/Japan Meteorological Agency (JMA) Climate Data Assimilation System (JCDAS, *Onogi et al*. [2007]).

3. Methods

We use a Lagrangian particle dispersion model, FLEXible PARTicle dispersion model (FLEXPART) [*Stohl et al*., 1998, 2005] with a high-resolution ($0.1° \times 0.1°$) emission inventory (ODIAC) to simulate X_{CO2} abundance ($\Delta X_{CO2,sim}$) caused by local emissions from fossil fuel combustion at all satellite observation locations. Based on these model estimates, we select satellite observations influenced substantially by fossil fuel emissions ($\Delta X_{CO2,sim} > 0.1$ ppm). The threshold of 0.1 ppm for defining observations influenced by fossil fuel emissions was selected by examining the average simulated fossil fuel abundance ($\Delta X_{CO2,sim}$) over major desert areas (where anthropogenic activity is low) across the world, which was found to be below 0.1 ppm (see Text S2 and Table S1 in the supporting information). Observed enhancements ($\Delta X_{CO2,obs}$) were computed as deviations from the background defined as a mean of all "clean" (clean—observations that are not influenced by emission from fossil fuel) measurements in the area around the observation point (average of observations with low contribution from fossil fuel sources in $10° \times 10°$ boxes). A $2° \times 2°$ averaged $\Delta X_{CO2,obs}$ and $\Delta X_{CO2,sim}$ is given in Figures 1a and 1b, respectively.

Since X_{CO2} comprises contributions from fossil fuel combustion, biomass burning, and terrestrial biospheric fluxes, model-based estimates for contributions by biospheric fluxes and biomass burning emissions, typically small compared to $\Delta X_{CO2,obs}$ values, are subtracted from the observations. These observed enhancements may contain contributions from other sources such as emissions from biofuel use [*Wang et al*., 2013]. To reduce the stochastic errors of the order of 2 ppm [*Yoshida et al*., 2013] associated with each individual satellite observation,

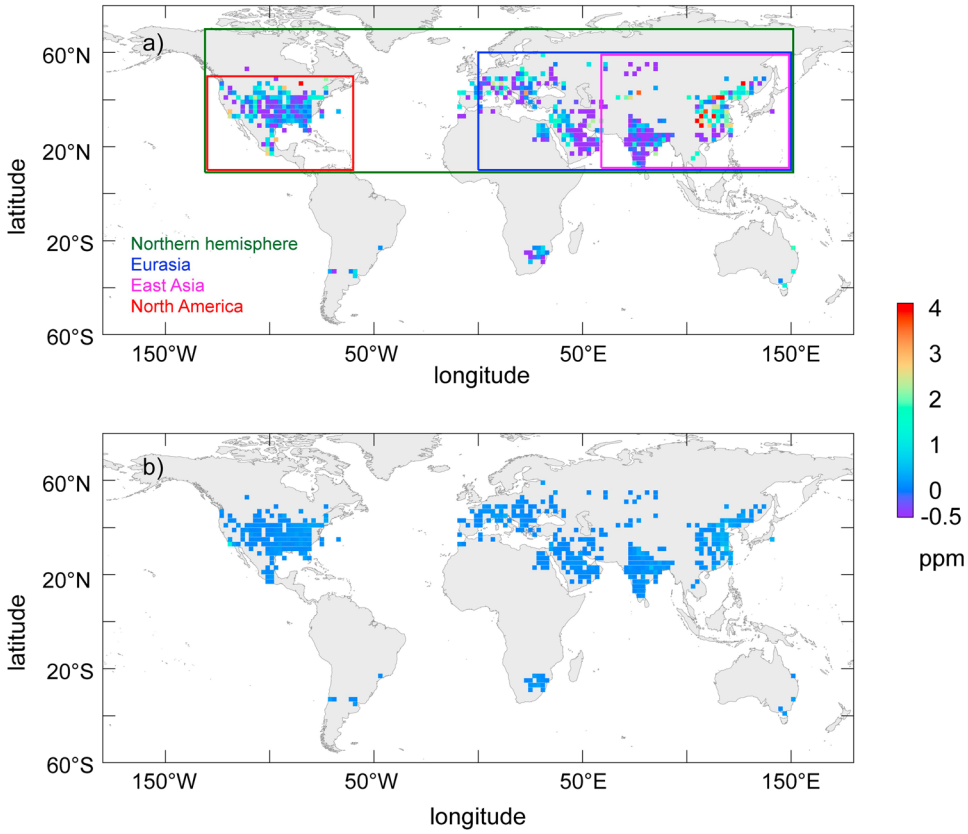

Figure 1. Observed and simulated total column CO_2 with significant fossil fuel signature averaged over 2° × 2° grid. (a) GOSAT-deduced fossil fuel enhancements in X_{CO2} ($\Delta X_{CO2,obs}$; color shading; ppm) averaged over 2° × 2° grid where atleast 10 observations exist for 2009–2012. The macro regions—East Asia (10–60°N, 60–150°E), Eurasia (10–60°N, 0–150°E), North America (10–50°N, 130–60°W), and the Northern Hemisphere (10–70°N, 130°W–150°E)—used for regional regression between modeled and observed ΔX_{CO2} are shown by colored rectangles. Overlapping boundaries are drawn with 1° offset for visual clarity. (b) Simulated fossil fuel enhancements in X_{CO2} ($\Delta X_{CO2,sim}$; color shading; ppm).

we aggregate the observed ($\Delta X_{CO2,obs}$) and simulated ($\Delta X_{CO2,sim}$) anomalies into 0.2 ppm bins based on simulated enhancements. To relate the fossil fuel CO_2 emission inventory to the observed enhancements, we perform linear regression [*Brown*, 2014] (weighted by standard error in mean $\Delta X_{CO2,obs}$) of observed against simulated enhancements. The regression is carried out for the enhancement range 0.2–1 ppm since the weak signals (<0.2 ppm) are more strongly affected by fluxes from sources other than fossil fuel emissions. The upper limit is selected based on the standard error in the bin average (see discussion on error estimate in the supporting information), which increases with decreasing number of observations (see Figures S2b and S3). We exclude enhancement bins where we have less than around 50 observations, considering the growing error in the mean value (Figure S2a). Most of the observations (approximately 99%) influenced by fossil fuel emissions fall below this upper limit. In ideal condition, the slope of the weighted linear regression (S_r) corresponds to a correction factor by which the inventory-based emissions would need to be scaled in order to bring observed and simulated values in agreement.

3.1. Lagrangian Simulation of CO_2 Transport

We have calculated CO_2 transport for all GOSAT scans for a period from June 2009 to December 2012. Ten thousand virtual particles were released from each receptor position (the geographic locations of GOSAT observations) and transported 2 days backward in time with the three-dimensional wind field and using parameterizations for turbulence and convection. We used the Japan Meteorological Agency (JMA) Climate Data Assimilation System (JCDAS) [*Onogi et al.*, 2007] reanalysis at 1.25° spatial and 6-hourly temporal resolution. The time integral of particle density below the mixing height in an emission grid cell gives the sensitivity of the trace gas mixing ratio at the receptor to the emission in that cell [*Ganshin et al.*, 2012].

The CO_2 mixing ratio at the observation location is then obtained as the area integral of the emission sensitivity multiplied by the CO_2 flux [*Lin et al*., 2003; *Seibert and Frank*, 2004; *Ganshin et al*., 2012]. Spatial resolution of the surface fluxes of 0.1° was chosen to match the GOSAT observation footprint of approximately 10 km (see Figure S4).

3.2. ΔX_{CO2} From GOSAT

GOSAT X_{CO2} observations (in parts per million) are used for estimating the X_{CO2} enhancements due to fossil fuel emissions (denoted as $\Delta X_{CO2,obs}$) relative to surrounding cleaner areas. For this, we consider the observations where model-simulated enhancements due to fossil fuel emissions (denoted as $\Delta X_{CO2,sim}$) exceed 0.1 ppm to have fossil CO_2 signature (see Text S2), and the rest of the observations as clean background. To extract the fossil component of X_{CO2}, we subtract the model-simulated contributions by the biospheric and biomass burning fluxes ($\Delta X_{CO2,bio}$ and $\Delta X_{CO2,fire}$) from the observed X_{CO2} values:

$$X_{CO2,cor} = X_{CO2,obs} - \Delta X_{CO2,bio} - \Delta X_{CO2,fire} \quad (1)$$

We assume that the influence of terrestrial biospheric and biomass burning fluxes is largely removed by this procedure, and any residual influences from $\Delta X_{CO2,bio}$ and $\Delta X_{CO2,fire}$ and model errors are not correlated with the enhancements due to the fossil fuel emission of interest. We then estimate the X_{CO2} enhancement relative to the clean surrounding observations as the difference between observed value and a clean background value $X_{CO2,bg}$.

$$\Delta X_{CO2,obs} = X_{CO2,cor} - X_{CO2,bg} \quad (2)$$

In order to estimate the background mixing ratios, $X_{CO2,bg}$, we defined rectangular regions of $10° \times 10°$ globally and took the monthly means of corrected observations ($X_{CO2,cor}$) for locations corresponding to simulated $\Delta X_{CO2,sim} < 0.1$ ppm (where there are more than 16 clean observations) which are considered clean pixels in each region. To relate the observed enhancements ($\Delta X_{CO2,obs}$) to the simulated enhancements ($\Delta X_{CO2,sim}$), we sorted all paired values into 0.2 ppm bins based on simulated values of $\Delta X_{CO2,sim}$. Subsequently, we averaged both the model-simulated and observation-deduced enhancements for each 0.2 ppm bin. This procedure was done to reduce the stochastic error associated with each individual observation. Resulting data are used in regression analysis as shown in Figure 2.

4. Results

In our analysis it is required that we have a large number of individual observations of both emission-influenced and clean background X_{CO2}, as it is difficult to distinguish between signal and noise for smaller regions containing few observations around strong CO_2 sources. Due to this, we have selected large regions and a long time period to include a sufficient number of observations in the analysis. Therefore, we first analyze the data globally and over the Northern Hemisphere and, for analysis on continental scale, over three large regions with significant CO_2 emissions from fossil fuel burning but with different economic development: East Asia, Eurasia, and North America (colored rectangles in Figure 1a). We did not isolate Europe from Eurasia because the number of observations for Europe alone is relatively low. When we apply regression of the aggregated observed enhancements against the simulated enhancements, we found a good linear relationship globally and for the Northern Hemisphere (Figure 2).

For the global case, observed and simulated enhancements showed good agreement with a slope S_r of 1.21 ± 0.21 ($p < 0.05$) (Figure 2a). The error in the slope accounts for both the uncertainty in the enhancements (combined effect of noisy observational data, errors in background estimate, and dispersion model) and deviation of enhancements from regression line. In the Northern Hemisphere case, the S_r value is 1.12 ± 0.22 ($p < 0.05$) (Figure 2b), and for Eurasia we found an S_r value of 1.24 ± 0.27 ($p < 0.05$) (Figure 2c). In the case of these three large domains, though the S_r values differ from unity (within the uncertainty range), the observed and simulated enhancements are very close to the "identity line" (line where $\Delta X_{CO2,obs}$ and $\Delta X_{CO2,sim}$ are equal; grey dashed lines in Figure 2) suggesting that the emissions from strong point sources are well captured in the model. Figure S1 depicts the ratio between $\Delta X_{CO2,obs}$ and $\Delta X_{CO2,sim}$ which also suggests that the observed and simulated enhancements agree well in these regions. However, when we perform our analysis for East Asia, the S_r value is similar (1.22 ± 0.32, ($p < 0.05$); Figure 2d), but the regression line

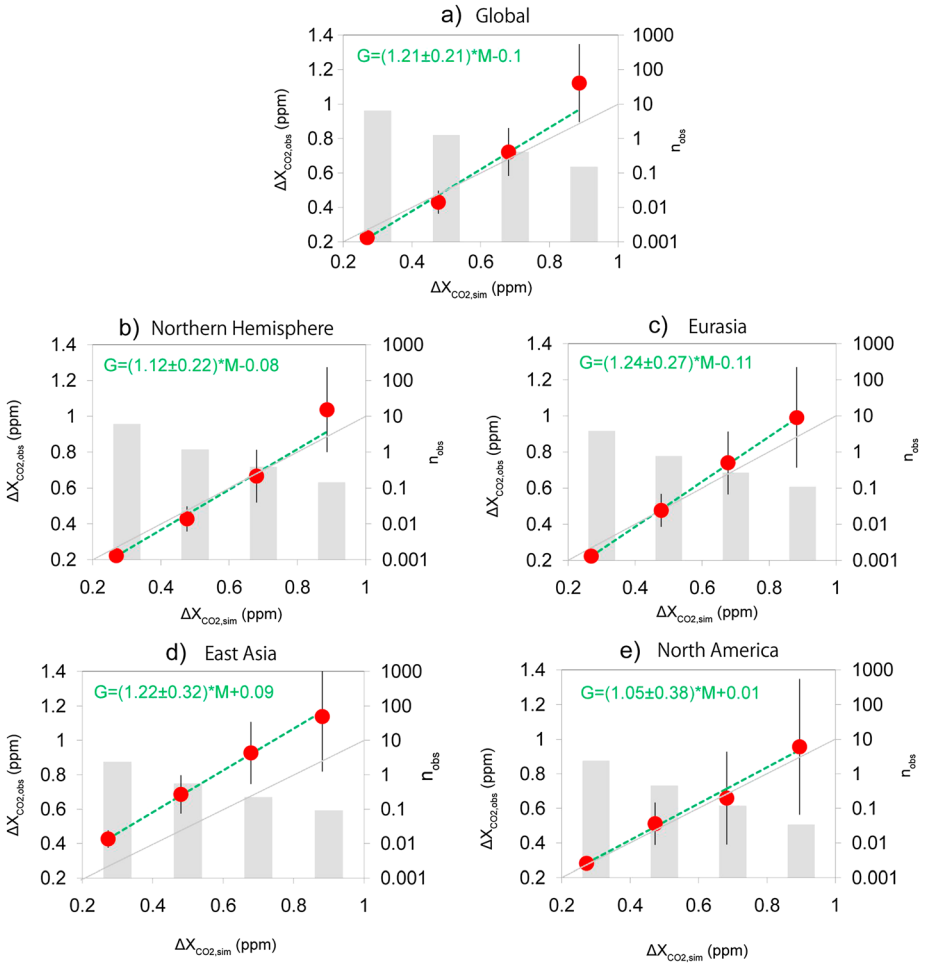

Figure 2. Mean observed ($\Delta X_{CO2,obs}$) versus simulated ($\Delta X_{CO2,sim}$) enhancements in 0.2 ppm bins for (a) Globe, (b) Northern Hemisphere, (c) Eurasia (d) East Asia, and (e) North America. Vertical thin lines show the standard error of the mean observed enhancements. Standard errors in the binning of simulated values are smaller than the symbol size. The grey dashed line is the identity line. The error-weighted regression between the modeled and observed X_{CO2} enhancements is shown as the green dashed line. The regression equation is shown at the top left of each panel (G, GOSAT; M, Model). The grey bars give the number of observations in thousands (right vertical axis, logarithmic scale; read n_{obs} as $n_{obs} \times 10^3$) in each enhancement bin.

has a large offset from the identity line (identity line outside observation uncertainty range)—indicating sizable differences between the mean simulated ($\Delta X_{CO2,sim}$) and observed enhancements ($\Delta X_{CO2,obs}$). Figure S1 shows that the ratio between the observed and simulated enhancements ($\Delta X_{CO2,obs}/\Delta X_{CO2,sim}$) is consistently greater than unity for East Asia for the analysis window 0.2–1 ppm. For North America, we find an S_r value of 1.05 ± 0.38 ($p < 0.1$), showing good match between model and observations though the uncertainty is largest among the five regions due to the smaller number of observations (Figure 2e). Sensitivity tests have shown that the model-based corrections for influences from biospheric and biomass burning do not affect the S_r value significantly (see Table S2).

The aforementioned differences over East Asia suggested by regression analysis imply that inventory emissions are lower than needed to match the observations. This region is known for large differences between fossil fuel CO_2 emission inventories [*Guan et al.*, 2012; *Liu et al.*, 2015]. For example, a recent study [*Guan et al.*, 2012] estimated Chinese provincial total CO_2 emissions of 9.08 Gt yr^{-1} for 2010, which is 1.4 Gt yr^{-1} more than the national report. *Liu et al.* [2015] have reported that the Chinese energy consumption was 10% higher in their revised estimate than the Chinese national statistics. Though they have revised the emission factors for coal burned in China and estimated lower net emissions than other established CO_2 emission inventories, these

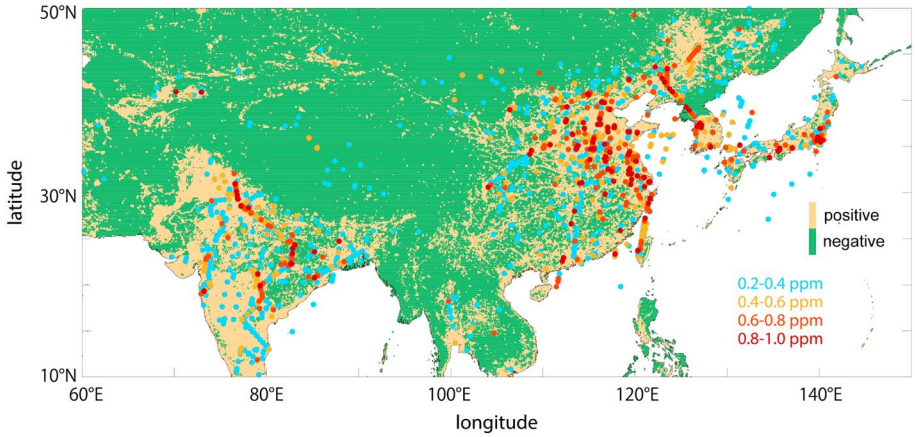

Figure 3. Simulated enhancements for East Asian domain and comparison between ODIAC and Emission Database for Global Atmospheric Research (EDGAR). Observation locations (colored dots) corresponding to 0.2–1 ppm X_{CO2} abundance ($\Delta X_{CO2,sim}$) over East Asian domain. The color shading over the map shows the difference between ODIAC and EDGAR inventories for the years 2008–2010 (yellow ODIAC higher, green ODIAC lower).

aspects have been questioned by some recent studies [e.g., *Olivier et al*., 2015]. Another study [*Zhao et al*., 2012] recompiling the Chinese CO_2 emissions using provincial level energy statistics revealed that CO_2 emission from fossil fuel and cement production showed notable differences with generally accepted estimates (e.g., 5–10% higher than CDIAC [*Boden et al*., 2013] during 2005–2009). These uncertainties in the national total CO_2 emissions are propagated to derived global emission data sets and our model simulations. Figure 3 shows that the observations corresponding to simulated enhancements in the range of 0.2 to 1 ppm in East Asia are largely clustered over eastern China and India where fossil fuel emissions and the uncertainties in them are high (details in Figure 3). The discrepancy between simulated and observed X_{CO2} abundance (22%) and its uncertainty (32%) over East Asia are comparable to the uncertainties (~15%) associated with fossil fuel CO_2 emission over this region [e.g., *Zhao et al*., 2012].

To reveal the localized areas with strong emissions that are accompanied by statistically significant observed enhancements in X_{CO2}, we repeated similar analysis to observations where simulated enhancements are higher than 1 ppm and selected $1° \times 1°$ regions with at least five such observations inside. We found several such locations over the globe (Table 1). The observation and model values for those locations are statistically consistent, i.e., difference between the mean observed and simulated enhancements lie within the magnitude of the estimated observation error. Despite possible model errors and contamination of the GOSAT retrievals by aerosols of urban and industrial origin, root-mean-square of the model-observation difference

Table 1. Average Fossil Fuel Enhancements in X_{CO2} Averaged Over Selected $1° \times 1°$ Grid Cells for Model ($\Delta X_{CO2,sim}$) and Observation ($\Delta X_{CO2,obs}$)[a]

City (Country)	Location	$\Delta X_{CO2,obs}$	$\Delta X_{CO2,sim}$	σ_{obs}	n_{obs}	SE
Bilaspur and Corba (India)	82.5°E, 22.5°N	0.98	1.23	2.66	17	0.65
Bhubaneshwar (India)	85.5°E, 20.5°N	1.04	1.66	2.91	17	0.70
Sonhat (India)	82.5°E, 23.5°N	0.60	1.48	2.23	12	0.64
New Delhi (India)	77.5°E, 28.5°N	2.44	1.72	4.27	7	1.61
Xi'an (China)	108.5°E, 34.5°N	3.25	1.91	4.53	6	1.85
Yancheng (China)	119.5°E, 33.5°N	1.96	1.44	2.57	5	1.15
Shanghai (China)	120.5°E, 31.5°N	1.55	1.81	3.45	5	1.54
Beijing and Tianjin (China)	116.5°E, 39.5°N	1.85	2.07	2.62	10	0.83
Shanxi (China)	112.5°E, 37.5°N	2.34	1.48	3.19	7	1.21
Tianjin (China)	117.5°E, 39.5°N	2.09	1.54	2.29	7	0.86
Los Angeles (USA)	118.5°W, 33.5°N	2.75	1.60	2.86	8	1.01
Yangpyeong (Korea)	127.5°E, 37.5°N	1.79	2.14	2.30	6	0.94

[a]The central longitude and latitude of selected $1° \times 1°$ grids are given as Location. σ_{obs} and n_{obs} are the standard deviation and number of observations available in the grid cell, respectively, and SE is the standard error. Grid boxes are selected with SE less than 2 and n_{obs} greater than 4.

divided by the observation error is less than one (0.72), which indicates agreement between model and observations is statistically valid. Locations listed in Table 1 do not necessarily represent the highest emissions around the globe but are typically places where high emissions are accompanied by stagnant meteorological conditions, which favor local accumulation of CO_2 and thus elevated X_{CO2}, which is more easily observed. Furthermore, there are more observations over locations with long periods of clear-sky weather, favoring successful observation by GOSAT. Most of the locations are in India and China, with one each in the USA and Korea.

In India, we observed large enhancements at locations over the eastern part of the Gangetic Plain where the population and fossil fuel CO_2 emissions are large, which conform to the geographical locations of observations of X_{CO2} [*Reuter et al*., 2014] enhancements (or other pollutants, e.g., NO_x [*Richter et al*., 2005]) reported elsewhere. With the exception of Shanghai and Beijing, the observed enhancements for all Chinese locations were larger than the simulated ones. This is in agreement with previous studies [*Wang et al*., 2013] (overestimation of emission over large urban areas) and the results obtained from the regression analysis for East Asia as a whole (Figure 2d). The mean observed enhancement for Los Angeles (2.75 ± 1.01 ppm) is comparable with the results from another GOSAT-based study by *Kort et al*. [2012] (3.2 ± 1.5 ppm) covering the early part of this study period.

5. Conclusion

Several recent studies have shown the capability of observing the X_{CO2} abundance in the atmosphere due to large sources such as power plants and large cities. Our study is an attempt to analyze satellite observations of atmospheric CO_2 at global or subcontinental scales to attribute to emission from large sources. We found that the emission inventory-based X_{CO2} abundance and satellite observed abundance agree well over large regions where we have sufficient number of observations of polluted sites. The large observation-model mismatches over East Asia imply that the fossil fuel emission estimates by inventory from these regions likely to be below what is suggested by GOSAT-observed abundance over this region. This result is important, particularly in the context of the recent reports about the unaccounted fuel use in China by many researchers.

We found that with the precision and number of GOSAT observations, it is possible to monitor emissions from strong CO_2 sources such as power plants and megacities for regions with elevated CO_2 column abundance in the range of 0.2 to 1 ppm. Improving the accuracy and extending the spatial coverage of this analysis should be possible with a larger number of satellite observations, preferably with a smaller observation footprint (spectrometer's instantaneous field of view) around intense sources. Our results indicate that observations from GOSAT and other satellite such as Orbiting Carbon Observatory 2 [*Crisp et al*., 2004] can be used to detect fossil fuel signatures over large and consistently emitting regions globally and that satellite observations combined with our analysis method provide a promising tool to monitor CO_2 emissions from fossil fuel use and thus to verify bottom-up inventories of these emissions.

Acknowledgments
The authors are grateful to the GOSAT project at the National Institute for Environmental Studies, Japan, for support and providing the GOSAT Level 2 X_{CO2} data. The supercomputer facility and GOSAT Research Computation Facility at the National Institute for Environmental Studies are acknowledged for enabling the simulations. Study was supported by grant 2-1401 of Environment Research and Technology Development Fund, Ministry of Environment Japan. The two anonymous reviewers are gratefully acknowledged.

References

Andres, R. J., et al. (2012), A synthesis of carbon dioxide emissions from fossil-fuel combustion, *Biogeosciences*, *9*, 1845–71, doi:10.5194/bg-9-1845-2012.

Boden, T., G. Marland, and R. Andres (2013), *Global, Regional, and National Fossil-Fuel CO_2 Emissions*, Carbon Dioxide Information Analysis Center, Oak Ridge Nat. Lab., Ridge, Tenn.

Bovensmann, H., M. Buchwitz, J. P. Burrows, M. Reuter, T. Krings, K. Gerilowski, O. Schneising, J. Heymann, A. Tretner, and J. Erzinger (2010), A remote sensing technique for global monitoring of power plant CO_2 emissions from space and related applications, *Atmos. Meas. Tech.*, *3*, 781–811.

Brown, J. D. (2014), *Linear Models in Matrix Form: A Hands-On Approach for the Behavioral Sciences*, Springer, Switzerland.

Crisp, D., et al. (2004), The Orbiting Carbon Observatory (OCO) mission, *Adv. Space Res.*, *34*, 700–709.

Duren, R. M., and C. E. Miller (2012), Measuring the carbon emissions of megacities, *Nat. Clim. Change*, *2*, 560–562.

Friedl, M. A., et al. (2002), Global land cover mapping from MODIS: Algorithms and early results, *Remote Sens. Environ.*, *83*, 287–302.

Ganshin, A., et al. (2012), A global coupled Eulerian-Lagrangian model and 1 × 1 km CO_2 surface flux dataset for high-resolution atmospheric CO_2 transport simulations, *Geosci. Model Dev.*, *5*, 231–243.

Guan, D. B., Z. Liu, Y. Geng, S. Lindner, and K. Hubacek (2012), The gigatonne gap in China's carbon dioxide inventories, *Nat. Clim. Change*, *2*, 672–675, doi:10.1038/nclimate1560.

Ito, A. (2010), Changing ecophysiological processes and carbon budget in East Asian ecosystems under near-future changes in climate: Implications for long-term monitoring from a process-based model, *J. Plant Res.*, *123*, 577–588.

Kaiser, J. W., et al. (2012), Biomass burning emissions estimated with a global fire assimilation system based on observed fire radiative power, *Biogeosciences*, *9*, 527–554.

Kort, E. A., C. Frankenberg, C. E. Miller, and T. Oda (2012), Space-based observations of megacity carbon dioxide, *Geophys. Res. Lett.*, *39*, L17806, doi:10.1029/2012GL052738.

Kuze, A., H. Suto, M. Nakajima, and T. Hamazaki (2009), Thermal and near infrared sensor for carbon observation Fourier-transform spectrometer on the Greenhouse Gases Observing Satellite for greenhouse gases monitoring, *Appl. Opt.*, *48*, 6716–6733.

Lin, J. C., C. Gerbig, S. C. Wofsy, A. E. Andrews, B. C. Daube, K. J. Davis, and C. A. Grainger (2003), A near-field tool for simulating the upstream influence of atmospheric observations: The Stochastic Time-Inverted Lagrangian Transport (STILT) model, *J. Geophys. Res.*, *108*(D16), 4493, doi:10.1029/2002JD003161.

Liu, Z., et al. (2015), Reduced carbon emission estimates from fossil fuel combustion and cement production in China, *Nature*, *524*, 335–338.

National Research Council (2010), *Verifying Greenhouse Gas Emissions: Methods to Support International Climate Agreements*, Natl. Acad. Press, Washington, D. C.

Nisbet, E., and R. Weiss (2010), Top-down versus bottom-up, *Science*, *328*, 1241–1243, doi:10.1126/science.1189936.

Oda, T., and S. Maksyutov (2011), A very high-resolution (1 km × 1 km) global fossil fuel CO_2 emission inventory derived using a point source database and satellite observations of nighttime lights, *Atmos. Chem. Phys.*, *11*, 543–556.

Olivier, J. G. J., et al. (2015), Trends in global CO2 emissions; 2015 Report The Hague: PBL Netherlands Environmental Assessment Agency; European Commission, Ispra.

Onogi, K., et al. (2007), The JRA-25 Reanalysis, *J. Meteorol. Soc. Jpn.*, *85*, 369–432.

Reuter, M., M. Buchwitz, A. Hilboll, A. Richter, O. Schneising, M. Hilker, J. Heymann, H. Bovensmann, and J. P. Burrows (2014), Decreasing emissions of NO_x relative to CO_2 in East Asia inferred from satellite observations, *Nat. Geosci.*, *7*, 792–795, doi:10.1038/ngeo2257.

Richter, A., J. P. Burrows, H. Nüβ, C. Granier, and U. Niemeier (2005), Increase in tropospheric nitrogen dioxide over China observed from space, *Nature*, *437*, 129–132.

Saito, M., A. Ito, and S. Maksyutov (2014), Optimization of a prognostic biosphere model for terrestrial biomass and atmospheric CO_2 variability, *Geosci. Model Dev.*, *7*, 1829–1840.

Seibert, P., and A. Frank (2004), Source-receptor matrix calculation with a Lagrangian particle dispersion model in backward mode, *Atmos. Chem. Phys.*, *4*, 51–63, doi:10.5194/acp-4-51-2004.

Stohl, A., M. Hittenberger, and G. Wotawa (1998), Validation of the Lagrangian particle dispersion model FLEXPART against large-scale tracer experiment data, *Atmos. Environ.*, *32*, 4245–4264.

Stohl, A., C. Forster, A. Frank, P. Seibert, and G. Wotawa (2005), Technical note: The Lagrangian particle dispersion model FLEXPART version 6.2, *Atmos. Chem. Phys.*, *5*, 2461–2474.

Wang, R., et al. (2013), High-resolution mapping of combustion processes and implications for CO_2 emissions, *Atmos. Chem. Phys.*, *13*, 5189–5203.

Yokota, T., Y. Yoshida, N. Eguchi, Y. Ota, T. Tanaka, H. Watanabe, and S. Maksyutov (2009), Global concentrations of CO_2 and CH_4 retrieved from GOSAT: First preliminary results, *SOLA*, *5*, 160–163.

Yoshida, Y., et al. (2013), Improvement of the retrieval algorithm for GOSAT SWIR X_{CO2} and XCH_4 and their validation using TCCON data, *Atmos. Meas. Tech.*, *6*, 1533–1547.

Zhao, Y., C. P. Nielsen, and M. B. McElroy (2012), China's CO_2 emissions estimated from the bottom up: Recent trends, spatial distributions, and quantification of uncertainties, *Atmos. Environ.*, *59*, 214–223.